Excimer-laser-induced melting and solidification of monocrystalline Si: Equilibrium and nonequilibrium models

R. Černý
Faculty of Civil Engineering, Czech Technical University, Thákurova 7, 166 29 Prague 6, Czechoslovakia

R. Šášik, I. Lukeš, and V. Cháb
Institute of Physics, Czechoslovak Academy of Sciences, Na Slovance 2, 180 40 Prague 8, Czechoslovakia
(Received 14 December 1990; revised manuscript received 29 April 1991)

A theoretical description of ArF-excimer-laser-induced thermal processes in monocrystalline silicon is presented. Two models are given consideration: (1) the equilibrium model, involving a condition of the local thermodynamic equilibrium, and (2) the nonequilibrium model, considering a functional relationship between the temperature of the solid-liquid interface and the interfacial velocity. Comparison of both models reveals only small differences in the resulting molten layer thickness and melt duration but significant differences in the temperature fields and the resolidification dynamics. Confrontation of both models with experimental results strongly favors the nonequilibrium model, which—in principle—can explain the Si(100) surface structure modifications by ArF-excimer-laser irradiation.

I. INTRODUCTION

Processes of laser-controlled melting, recrystallization, and ablation of silicon represent a significant topic in the research of the laser-solid interaction. Recently published papers (see, e.g., Refs. 1–3) sustained important advantages of the excimer-laser radiation in comparison with the longer-wavelength light arising mostly from much stronger absorption and only a slight temperature dependence of the optical properties of Si in the UV region.

The need to describe these phenomena quantitatively gave rise to a melting model of the laser processing of materials (see Ref. 4, and references therein, for example) built in terms of equilibrium thermodynamics, which we will refer to as the equilibrium (EQ) model. However, there is a large volume of experimental evidence proving that laser melting of materials may be a highly nonequilibrium process: the authors of Ref. 5–7 reported amorphization of (100) silicon if the regrowth velocity reaches $\sim 15-20$ m. s^{-1}.

In this paper we introduce a model involving interfacial kinetics, which we will refer to as the nonequilibrium (NE) model. Our attention and computer modeling will be devoted to the description of much subtler phenomenon on excimer-laser-irradiated silicon described in detail in Ref. 8: An unusual "bulklike" (1×1) surface structure prepared on (100)-oriented silicon by ArF excimer-laser irradiation under ultrahigh-vacuum conditions. The fact that the initial sample temperature strongly affects the resulting surface structure [(2×1) or (1×1)] also suggests the necessity to put in place a proper theoretical model of laser-controlled phase changes in Si.

The EQ model is mathematically formulated as a classical Stefan problem (see, e.g., Ref. 9). This approach—customarily assuming that the introduction of an interfacial kinetics into the model is unnecessary—is rather adequate for slow processes. However, the motion of the solid-liquid interface can be so fast in some cases that this assumption is no longer valid and strong undercooling or overheating of the material in various phases must be considered.

Previously published models dealing with nonequilibrium phase transitions (see, e.g., Ref. 10) are based on enthalpy considerations. There the position of the phase interface does not appear explicitly; it is derived from the local enthalpy contents of the sample. In this paper, the condition of the local thermodynamic equilibrium at the phase interface is replaced with the interface response function and the phase interface itself is treated explicitly as a position of the moving boundary between the solid and liquid phases.

From a physical point of view, the nonequilibrium models are evidently more adequate for a description of such dynamic processes like laser-induced melting and solidification. Their disadvantage, however, lies in the fact that they employ a number of additional material parameters. One of the objectives of this paper is, therefore, a comparison of the applicability of the equilibrium and the nonequilibrium models in a real experimental situation (Ref. 8).

II. MATHEMATICAL FORMULATION

Let us consider the equilibrium model (i.e., the isothermal one-dimensional Stefan problem) in the form[9]

$$\rho c_i \frac{\partial T}{\partial t}=\frac{\partial}{\partial x}\left[K_i \frac{\partial T}{\partial x}\right]+S(x,t) \quad in\ \Omega_i,\ i=l,s\ , \tag{1}$$

$$\rho L_{\rm eq}\dot{Z}(t)=K_s \frac{\partial T}{\partial x}\bigg|_{x=Z^+}-K_l \frac{\partial T}{\partial x}\bigg|_{x=Z^-}\ , \tag{2}$$

$$T(Z,t)=T_{\rm eq}\ , \tag{3}$$

$$\left.\frac{\partial T}{\partial x}\right|_{x=0^+}=0 , \tag{4}$$

$$T(D,t)=T_0 , \tag{5}$$

$$T(x,0)=T_0 , \tag{6}$$

where ρ is the density, c_i is the specific heat, K_i is the thermal conductivity, $L_{\rm eq}$ is the latent heat, t equals time, x is the space variable, $Z(t)$ is the location of the moving boundary between the solid and liquid phases, $\dot{Z}(t)=dZ(t)/dt$, Ω_i is the space subdomain occupied by phase i, $\Omega_l+\Omega_s=\Omega,\Omega=\langle 0,D\rangle$. D is the size of the spatial domain (thickness of the sample). $T_{\rm eq}$ is the temperature of the equilibrium phase transition, the indices l and s denote liquid and the solid, respectively. The source term $S(x,t)$ in Eq. (1) describes the energy absorption of a laser pulse:

$$S(x,t)=(1-R)\alpha I_0(t)\exp(-\alpha x) , \tag{7}$$

where R is the reflectivity, α is the optical absorption coefficient, and $I_0(t)$ is the pulse intensity profile.

In the case of a nonequilibrium (nonisothermal) problem, condition (3) is replaced with a function expressing the dependence of the interface velocity on its temperature. The interface response function which was selected follows from a simple version of the Jackson-Chalmers theory[11]

$$\begin{aligned}\dot{Z}(T_x)&=f(T_z)\\&=C_1\exp(-Q/k_BT_z)\\&\quad\times 1-\exp[-L_p(1/T_z-1/T_{\rm eq})/k_B] .\end{aligned} \tag{8}$$

Here Q denotes the activation energy for self-diffusion in the liquid, L_p is the latent heat of fusion per particle, and C_1 is a material constant. In order to introduce a correct dependence of the latent heat L on the interface temperature T_z into (2), we perform the following quasiequilibrium considerations: If we cool a liquid silicon of a unit mass from melting point $T_{\rm eq}$ down to $T<T_{\rm eq}$, then manage to transform it into the solid at this nonequilibrium temperature by rapid drain of released heat $L(T)$, then slowly heat it up to the melting point $T_{\rm eq}$ and transform it into the liquid by equilibrium melting; the balance of consumed and released heat requires that

$$0=c_l(T-T_{\rm eq})-L(T)+c_s(T_{\rm eq}-T)+L_{\rm eq} .$$

Rearranging the terms of this equation,

$$L(T_Z)=L_{\rm eq}+(T_Z-T_{\rm eq})(c_l-c_s) , \tag{9}$$

where $L_{\rm eq}$ is the latent heat measured at the temperature $T_{\rm eq}$.

III. NUMERICAL SOLUTION

Let us consider the isothermal problem first. Landau's transformations

$$\zeta=\frac{x}{Z(t)},\quad x\in\langle 0,Z(t)\rangle \tag{10}$$

and

$$\xi=\frac{x-Z(t)}{D-Z(t)},\quad x\in\langle Z(t),D\rangle \tag{11}$$

transform (1) and (2) into

$$\rho c_l\left[\frac{\partial T}{\partial t}-\dot{Z}\frac{\zeta}{Z}\frac{\partial T}{\partial\zeta}\right]=\frac{1}{Z^2}\frac{\partial}{\partial\zeta}\left[K_l\frac{\partial T}{\partial\zeta}\right]+S(Z,\zeta,t)$$
$$\text{in } \Omega_l'=\langle 0,1\rangle , \tag{12}$$

$$\rho c_s\left[\frac{\partial T}{\partial t}-\dot{Z}\frac{1-\xi}{D-Z}\frac{\partial T}{\partial\xi}\right]=\frac{1}{(D-Z)^2}\frac{\partial}{\partial\xi}\left[K_s\frac{\partial T}{\partial\xi}\right]+S(Z,\xi,t)$$
$$\text{in } \Omega_s'=\langle 0,1\rangle , \tag{13}$$

$$\rho L_{\rm eq}\dot{Z}(t)=\frac{1}{D-Z}K_s\left.\frac{\partial T}{\partial\xi}\right|_{\xi=0^+}-\frac{1}{Z}K_l\left.\frac{\partial T}{\partial\zeta}\right|_{\zeta=1^-} , \tag{14}$$

and subdomains Ω_l, Ω_s are converted into two fixed-space intervals Ω_l', Ω_s'. The fact that the parameter $Z(t)$ now becomes an independent variable allows straightforward boundary tracking and convenient numerical solution of (12)–(14) (see Ref. 12).

The space discretization and the standard Galerkin-type finite-element procedure[13] give the following system of differential equations (see Ref. 12 for details):

$$\underline{P}(Z)\frac{\partial}{\partial t}\{T\}+\underline{H}(Z,\dot{Z})\{T\}+\{U(Z,t)\}+\{B(Z,\dot{Z})\}=\{0\}. \tag{15}$$

$\underline{P}(Z)$ and $\underline{H}(Z,\dot{Z})$ are square matrices, column vectors $\{T\}$, $\{U(Z,t)\}$, and $\{B(Z,\dot{Z})\}$ represent the temperature field, source term, and boundary conditions, respectively.

Let n be the number of points in the liquid and m be the number of points in the solid. Then

$$\{T\}=\langle T_{l1},\ldots,T_{l,n-1},T_{s1},\ldots,T_{sm}\rangle^T ,$$
$$T_{ln}\equiv T_{s1} .$$

The time discretization of Eq. (15) (see Ref. 13) gives the resulting set of algebraic equations

$$\bar{\underline{H}}(Z,\dot{Z})\{T\}_{t+\Delta t}=\bar{\underline{P}}(Z,\dot{Z})\{T\}_t-\{\bar{U}(Z,t)\}-\{B(Z,\dot{Z})\} , \tag{16}$$

where

$$\bar{\underline{H}}(Z,\dot{Z})=\tfrac{2}{3}\underline{H}(Z,\dot{Z})+\frac{1}{\Delta t}\underline{P}(Z) , \tag{17}$$

$$\bar{\underline{P}}(Z,\dot{Z})=\frac{1}{\Delta t}\underline{P}(Z)-\tfrac{1}{3}\underline{H}(Z,\dot{Z}) , \tag{18}$$

$$\{\bar{U}(Z,t)\}=\tfrac{1}{3}\{U(Z,t)\}_t+\tfrac{2}{3}\{U(Z,t)\}_{t+\Delta t} . \tag{19}$$

Δt is the length of a time element.

Conditions (3) and (4) that apply to the moving boundary are treated in the standard way: The condition of the local termodynamic equilibrium (3) is applied as a

Dirichlet-type condition for $T_{ln}=T_{s1}\equiv T_{eq}$, the Stefan condition (14) as the convergence criterion in the iteration procedure. The iteration process is designed as follows: (1) compute $\{T\}_{t+\Delta t}^{1}$ from (16) with $\dot{Z}=\dot{Z}_0$ and $Z=Z_0$, (2) compute $\dot{Z}_1$ from (14) as the first approximation to $\dot{Z}$, (3) compute $\{T\}_{t+\Delta t}^{k}$ from (16) with

$$\dot{Z}_k=(1-q)\dot{Z}_0+q\dot{Z}_{k-1},\quad q\in\langle 0,1\rangle ,$$

$$Z_k=Z_0+q\Delta t[\dot{Z}_0+q(\dot{Z}_{k-1}-\dot{Z}_0)/2] ,$$

(4) compute $\dot{Z}_{k+1}$ from (14) and make a test

$$\left|\frac{\dot{Z}_{k+1}-\dot{Z}_k}{1+\dot{Z}_k}\right|<\epsilon .$$

If this is true, accept the solution

$$\{T\}_{t+\Delta t}=\{T\}_{t+\Delta t}^{k} ,$$

$$\dot{Z}(t+\Delta t)=\dot{Z}_k ,$$

$$Z(t+\Delta t)=Z_0+\Delta t(\dot{Z}_0+\dot{Z}_k)/2 .$$

If not, put $\dot{Z}_{k-1}=\dot{Z}_k$ and go back to point (3).

The numeral solution of the nonisothermal problem is analogous with the presented one. The differences are in the application of the moving boundary conditions. The Stefan condition (14) is now involved in Eq. (16), hence, $\{B(Z,\dot{Z})\}$ has the form

$$\{B(Z,\dot{Z})\}=(0,\ldots,0,\rho f(T_Z)\times[L_{eq}+(c_s-c_l)T_{eq}],0,\ldots,0)^T . \quad (20)$$

where $f(T_Z)$ is the interface response function (8) and where there are $n-1$ initial zero terms and $m-1$ final zero terms. Condition (8) now becomes the convergence criterion, i.e., $\dot{Z}_{k+1}$ in point (4) of the iteration procedure is being computed from (8).

Being aware of the fact that both the specific heat and the thermal conductivity are temperature dependent; they are considered to be constant only within a small space-time finite element. In order to eliminate possible errors, the finite elements are designed so that halving their size results in the negligible change of the solution. The size D of the spatial domain is adjusted so that the choice of a higher value for D has no effect on the solution. This choice represents experiments with thick silicon samples.

Now we briefly discuss the technical matters, namely, the numerical performance of the finite element method and the convergence properties of the proposed iterative procedure: Generally, we find the finite-element method rewarding for its integral concept. In this case it is particularly important that it does not impose such severe restrictions on the size of the elements like, for example, the method of finite differences. It is sufficient that the grid points be dense enough to track satisfactorily the resulting temperature field, even though the source term $S(x,t)$ is strongly localized.

The iterative procedure introduced in point (3) proved to be convergent in every trial computation regardless of the size of parameter ϵ. Typically the quantity that is to be compared to ϵ reaches 10^{-2} after 2–3 iterative steps. It should be noted that each iterative step is approximately as time consuming as a single explicit time step without iterations. Therefore, it may appear more convenient not to allow multiple iterations within a single time step and let the program pass the iteration procedure (points 1–5) exactly once and employ a flexible step size control so that quantities like $\dot{Z}$, Z, or $T(0,t)$ would be changing by amounts which fall within specified limits. These two computational methods are virtually equivalent in terms of the outcoming results, as far as the corresponding time steps remain comparable. Further numerical aspects of the method have been described at length in Ref. 12.

IV. COMPARISON OF THE MODELS

We consider the following problem: The Si(100) surface is irradiated by ArF-excimer-laser pulse (193 nm, 10 ns FWHM). The energy density E of the pulse defined as

$$E=\int_0^{\infty} I_0(t)dt \quad (21)$$

is sufficient to melt the surface. The pulse shape $I_0(t)$ is triangular [see Figs. 1(a) and 1(b)]. The initial state of the silicon sample is solid, temperature $T(x,0)=T_0$ in the whole sample. There is no liquid phase until the surface temperature reaches T_{eq}. The problem of the appearing and disappearing of the liquid phase is treated in the same way as in Ref. 14: at the moment when the surface temperature reaches T_{eq}, a small layer of liquid phase is allowed to appear and the phase interface motion is driven by Eqs. (1)–(3) or (1), (2), and (8) according to the model used.

Thermodynamical and optical material parameters of the crystalline and liquid silicon are taken from Refs. 15 and 16, the thermal conductivity of the liquid silicon is evaluated from Wiedemann-Franz law (see Ref. 17). Values of constants appearing in the interface response function (8) that apply to (100)-oriented silicon have been accepted from Ref. 18.

Temperature fields and time dependences of the melt-front position and melting-and-solidification velocities were computed for both the EQ and the NE models under normal conditions ($T_0=293$ K) and the dependence of initial sample temperature. Results are presented in Figs. 1(a)–4(a) for the EQ model and in Figs. 1(b)–4(b) and 5 for the NE model. Of course, our EQ model results cannot, in principle, differ from those published by other authors due to the same system of equations and boundary conditions, but it is necessary to present them here for clear evaluation of the NE model.

Figures 1(a) and 1(b) represent computed surface temperatures $T(0,t)$ for various energy densities with initial sample temperature $T_0=293$ K. Differences between both models are relatively relevant in the maximum temperatures (in NE model, ~ 100 K higher) and in the temperatures in the cooling period (in NE model, ~ 70 K lower).

The displacement of the moving boundary ($Z(t)$, its appearance, and disappearance is shown in Figs. 2(a) and 2(b). The duration of the melting in the NE model is by 4 ns (i.e., 5%) longer than in the EQ model, the maximum

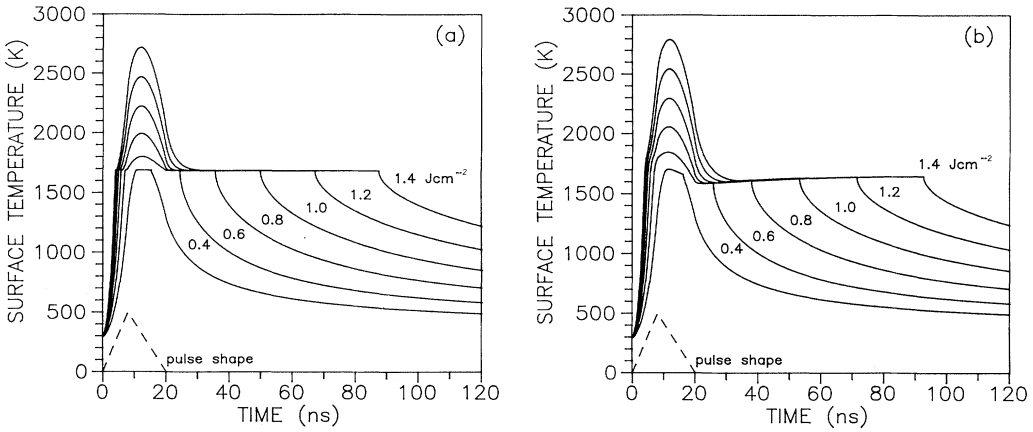

FIG 1. (a) The equilibrium model. Sample surface temperature vs time for energy densities E of the laser pulse from 0.4 to 1.4 J cm^{-2}. Initial sample temperature $T_0 = 293$ K. Pulse shape indicates the intensity profile $I_0(t)$. Fig. 1(b) The nonequilibrium model. The same as (a).

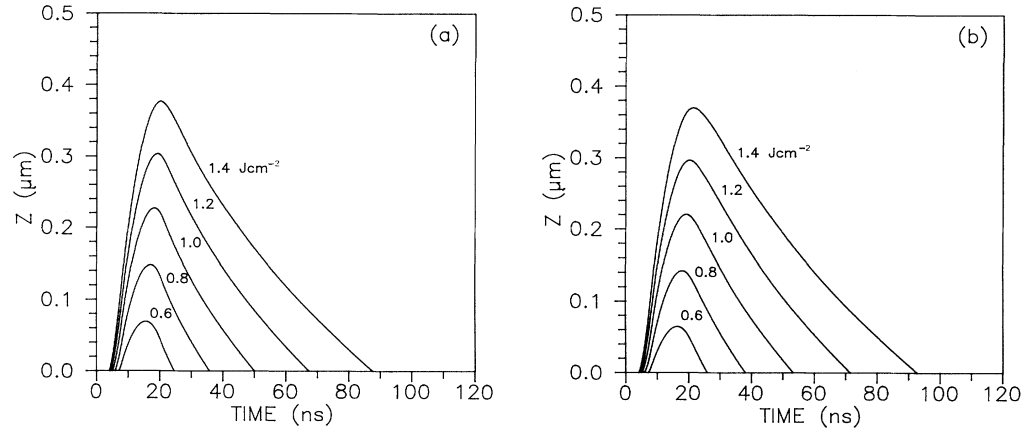

FIG. 2. (a) The equilibrium model. Melt-front penetration vs time for energy densities in the range from 0.6 to 1.4 J cm^{-2}. Initial sample temperature $T_0 = 293$ K. (b) The nonequilibrium model. The same as (a).

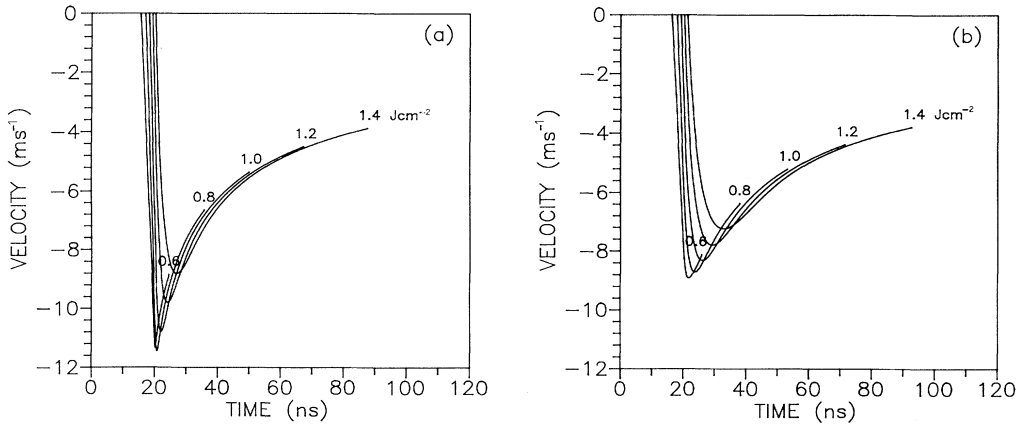

FIG. 3. (a) The equilibrium model. The resolidification velocity $\dot{Z}(t)$ of the phase interface vs time for energy densities from 0.6 to 1.4 J cm^{-2}. Initial sample temperature $T_0 = 293$ K. (b) The nonequilibrium model. The same as (a).

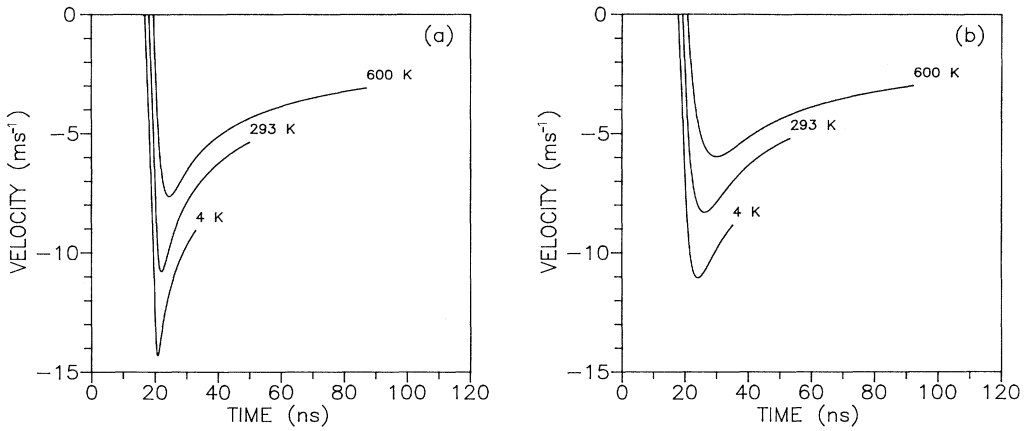

FIG. 4. (a) The equilibrium model. The resolidification velocity $\dot{Z}(t)$ of the phase interface vs time for initial sample temperatures T_0 ranging from 4 to 600 K. Energy density $E=1\ \mathrm{J\,cm^{-2}}$. (b) The nonequilibrium model. The same as (a).

thickness of the molten zone in the EQ model is by 0.01 μm (2%) higher.

Figures 3(a) and 3(b) represent the time dependence of the moving boundary velocity $\dot{Z}(t)$ during the resolidification. The maximum rate of growth predicted by the EQ model is considerably higher (more than 20%), but only in a short period of time (5–10 ns) after the end of the laser pulse; then the velocities in both models are in good agreement (better than 1%).

The influence of initial sample temperatures T_0 for $E=1\ \mathrm{J\,cm^{-2}}$, is shown in Figs. 4(a) and 4(b), and 5. Differences between the EQ and the NE model in solid-liquid interface velocities correspond with the results indicated by Figs. 3(a) and 3(b). The solidification rate increases rapidly with the lowering of temperature T_0—the regrowth velocity for $T_0=4$ K is about twice faster than that for $T_0=600$ K.

Figure 5 represents the time evolution of undercooling in the NE model during the solidification, which corresponds to Fig. 4(b). The maximum undercooling ΔT for $T_0=293$ K, $E=1\ \mathrm{J\,cm^{-2}}$ is 90 K and strongly increases with decreasing of the initial sample temperature and decreasing of the pulse energy density E [see Fig. 3(b)]. However, these maximum values are again a time-local matter (duration less than 10 ns) in time shortly after the end of the laser pulse. In the further solidification course, the undercooling values first rapidly decrease and then slowly approach certain more stabilized value.

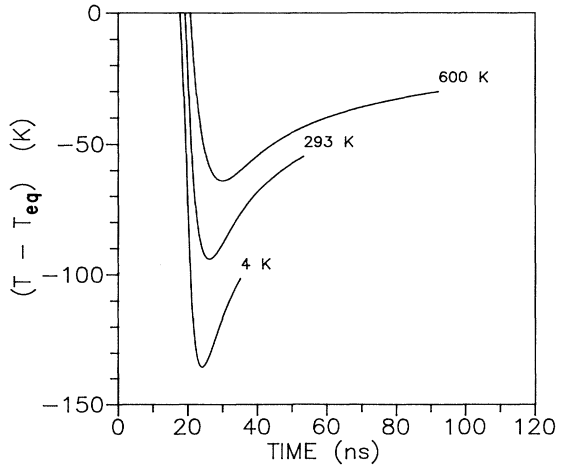

FIG. 5. The nonequilibrium model. Undercooling of the phase interface during the resolidification process for initial sample temperatures T_0 from 4 to 600 K. Energy density of the pulse $E=1\ \mathrm{J\,cm^{-2}}$.

V. DISCUSSION

Comparison of equilibrium and nonequilibrium theoretical models reveals that the differences in calculated values of the most often measured parameters—melt duration and maximum molten layer thickness—are too small to be resolved experimentally. This is the reason why the equilibrium model produces relatively good agreement with number of experimental data published to date.

Significant differences of both models become evident in the case of surface and solid-liquid interface temperature calculations. However, experimental determination of these quantities requiring sufficiently accurate temperature measurements with space and time resolution of about 0.1 μm and 10 ns, respectively, is not feasible at present.

The differences in maximum regrowth velocities reported by the models provide a good opportunity to verify their validity by measuring the regrowth velocity immediately after the end of a laser pulse. A description of the experimental method for such measurements based on an improved time-resolved reflectivity measurement technique will be given elsewhere.[19]

The role of the strong interfacial undercooling must be taken into account in the study of the metastable phases

formation. The priority of the NE model in such cases is evident. Our theoretical description of ArF excimer-laser-induced thermal processes on a mono-Si surface indicates the capability of the NE model to give an explanation of the observed surface structure modifications: The solidification rate [see Fig. 4(b)] and undercooling values (see Fig. 5) increase rapidly and reach nearly peak character with the lowering of the initial sample temperature. We suppose that these local extremes of undercooling in the time interval 15–20 ns (i.e., at the end of the laser irradiation) evoke the formation of lattice defects frozen at nonequilibrium concentration that stabilize observed Si(100)(1×1) surface structure.

The computed regrowth velocity always remained below 15 $m.s^{-1}$—the value critical for the amorphization of silicon. This is in accordance with experiments in Ref. 8 (for which the modeling was carried out), where amorphization was not encountered.

In fact, our NE model at present cannot handle amorphization nor recrystallization from amorphous phase because the contribution of the defects formation to the latent heat L is not known satisfactorily well. Therefore, the amorphization is not incorporated in the NE model. In order to extend the applicability to the NE model to amorphization, a necessary modification of formula (9) will be required. Still we should proceed with caution because formula (8) has been derived from molecular-dynamics simulations based on the Stillinger-Weber potential, the weak point of which is that it does not predict amorphization solely by rapid cooling of the liquid.[18]

VI. CONCLUSIONS

The evaluation of the equilibrium and nonequilibrium models of ArF-excimer-laser-induced thermal processes in mono-Si reveals only small or negligible differences between both models in quantities like maximum molten layer thickness and melt duration that are the most frequently measured quantities. Significant differences of both models consist in calculated temperature fields and resolidification velocity.

The priority of the NE model that provides information on the interfacial overheating and undercooling becomes evident when explaining the formation of metastable surface structures.

[1]G. Gorodetsky, J. Kanicki, T. Kazyaka, and R. L. Melcher, Appl. Phys. Lett. **46**, 547 (1985).
[2]G. B. Shinn, F. Steigerwald, H. Stiegler, R. Sauerbrey, F. K. Tittel, and W. L. Wilson, Jr., J. Vac. Sci. Technol. B **4**, 1273 (1986).
[3]F. Foulon, E. Fogarassy, A. Slaoui, C. Fuchs, S. Unamuno, and P. Siffert, Appl. Phys. A **45**, 361 (1988).
[4]R. F. Wood and G. E. Giles, Phys. Rev. B **23**, 2923 (1981).
[5]P. L. Liu, R. Yen, N. Bloembergen, and R. T. Hodgson, Appl. Phys. Lett. **34**, 864 (1979).
[6]R. Tsu, R. T. Hodgson, T. Y. Tan, and J. E. Baglin, Phys. Rev. Lett. **42**, 1356 (1979).
[7]A. G. Cullis, H. C. Weber, N. G. Chew, J. M. Poate, and P. Baeri, Phys. Rev. Lett. **49**, 219 (1982).
[8]J. Kubátová, V. Cháb, I. Lukeš, P. Jiříček, and F. Fendrych, Appl. Surf. Sci. **43**, 297 (1989).
[9]L. I. Rubinstein, *The Stefan Problem,* Vol. 27 of *AMS Translations of Mathematical Monographs* (American Mathematical Society, Providence, RI, 1971).
[10]R. F. Wood and G. A. Geist, Phys. Rev. B **34**, 2606 (1986).
[11]K. A. Jackson and B. Chalmers, Can. J. Phys. **34**, 473 (1956).
[12]R. Šášik and R. Černý, Comput. Phys. Commun. **64**, 241 (1991).
[13]O. C. Zienkiewicz, *The Finite Element Method in Engineering Science* (McGraw-Hill, London, 1971).
[14]R. Bonnerot and P. Jamet, J. Comput. Phys. **41**, 357 (1981).
[15]*Numerical Data and Functional Relationships in Science and Technology,* Landolt-Börnstein, New Series, Vol. 17 (Springer-Verlag, Berlin, 1982).
[16]G. E. Jellison, R. F. Wood, and G. E. Jellison, *Pulsed Laser Processing of Semiconductors,* edited by R. F. Wood, C. W. White, and R. T. Young (Academic, Orlando, 1984), Chaps. 3 and 4.
[17]C. Kittel, *Introduction to Solid State Physics* (Wiley, New York, 1976).
[18]M. D. Kluge and J. R. Ray, Phys. Rev. B **39**, 1738 (1989).
[19]I. Lukeš, R. Šášik, and R. Černý (unpublished).